Formation of Nanoliter Droplets in a Confined Microfluidic T-Shaped Junction: Formation Time and Droplet Volume

Yuxiang Zhang, Jing Fan and Liqiu Wang*

Department of Mechanical Engineering, The University of Hong Kong, Pokfulam Road, Hong Kong

Abstract: Nanoliter droplet formation in a confined T-shaped junction is analyzed in detail in virtue of an experimental visualization system with a high speed camera. The movement of the back interface of the tip of disperse phase penetrated into the continuous phase plays an important role in determining droplet formation time and droplet volume. A simple model of droplet formation time based on the analysis of droplet formation process is developed. Influences of continuous phase viscosity and interfacial tension on droplet formation time and droplet volume are concluded in terms of capillary number together with the mean velocity of continuous phase. It is found that both the capillary number and the flow rate ratio of disperse phase to continuous phase have strong impacts on determining droplet volume. Two empirical equations are derived from the model for predicting droplet formation time and droplet volume, respectively.

Keywords: Microchannel, T-shaped junctions, Nanoliter droplet, Droplet formation time, Droplet volume.

INTRODUCTION

Nanoliter droplets have extensive applications due to their little reagent consumtion and effective mixing in chemical synthesis and biochemical analysis [1-8]. Uniform nanoliter droplets dispersed into another immiscible fluid can form high quality monodisperse emulsions that are widely used in cosmetic, pharmaceutical and food industries [9-11]. A microfluidic device has the natural superiority to generate uniform nanoliter droplets in a controllable way because of its microscale characteristic dimensions and the laminar flow inside. The polydispersity, defined as the standard deviation of the droplet size distribution divided by the mean droplet size, can be as small as 1%. Many microfluidic structures have been demonstrated in generating uniform nanoliter droplets effectively including straight microchannel arrays [10-13], flow focusing devices [14-18], microcapillary tubes [19-21], and microchannel T-shaped junctions [22-28]. The principle of using microfluidic methods to generate nanoliter droplets is letting the disperse phase release droplets directly into the continuous phase under some instability where they meet together in a manner of either cross-flowing or co-flowing arrangement of the two flowing phases.

Most microchannel T-shaped junctions can be classified in to two groups according to their geometrical characteristics: unconfined T-shaped junctions and confined T-shaped junctions [29]. In an unconfined T-shaped junction, the continuous phase channel is much larger than the disperse phase channel such that the growing droplet can freely develop before detaching like in the membrane emulsification [23, 30, 31]. A force or torque balance model is normally developed to predict droplet volume, which is stated as a droplet detaches when all possible forces exerted on it reached equilibrium [25, 26]. In a confined T-shaped junction, however, the forming droplets are seriously confined by walls of continuous phase channel, and the force balance model is not applicable for predicting droplet volume [23, 27, 32, 33]. The failure may result from the inaccurate estimation of the forces involved in the droplet formation process that is seriously disturbed by the confinement of walls of continuous phase channel. There are many arguments over here about which parameters which contribute to the droplet formation most and how those parameters influence the droplet volume. Some researchers believe that, in confined T-shaped junctions, fluids properties have little impact on droplet volume when the capillary number is less than the order of 0.01, and the flow rate ratio of disperse phase to continuous phase is the only factor affecting the droplet volume for a specified T-shaped junction [27, 32]. In contrast, some other reports that the Capillary number representing the influence of fluids properties plays an important role in determining droplet volume, but the influence of flow rate ratio is not indicated [23, 33]. Moreover, few studies on droplet formation time in such confined T-shaped junctions are available. Therefore further examination of the droplet formation process in such confined microchannel T-shaped junctions is necessary and helpful for better utilization and manipulation of nanoliter droplets. In this work, we found that the dynamic movement of the back interface of the forming droplet plays an important role on droplet formation, and two empirical relations are worked out to conclude the influences of the mean velocities of disperse phase and continuous phase, the continuous phase viscosity, and the interfacial tension between continuous phase and disperse phase on droplet formation time and droplet volume.

EXPERIMENTS

Chemicals and Materials

Chemicals used in the preparation of microchannel T-shaped junction include hydrofluoric acid, ammonia fluoride, perchloric acid, ammonium cerium nitrate, sodium hydroxide, acetone, and ethanol (Tianjin Damao Chemical Reagent factory, China). All chemicals are of analytical grade. To generate nanoliter droplets, the disperse phase should avoid wetting channel walls of continuous phase in T-shaped junctions, which requires an aqueous solutions as continuous phase for naturally hydrophilic surface of microchannel walls of glass material used in our experiment. Aqueous solutions with different concentration of Tween 20 (Sigma-Aldrich) and glycerin (Tianjin Damao Chemical Reagent, China) are used as continuous phases, and hexadecane (Sigma-Aldrich) is selected as disperse phase. Here, Tween 20 is used to change the interfacial tension between hexadecane and deionized water, and glycerin is used to change the viscosity of continuous phase. Table **1** lists the measured values of interfacial tension and viscosity at room temperature. Each value is an average over three measurements. Interfacial tensions are measured by using a tensiometer (Cole-Parmer® Surface Tension Meter 20, Cole-Parmer Instrument Company, USA) with an accuracy of 0.25mN/m, and viscosities are measured by using a viscometer (SCHOTT-GERATE GmbH, Germany) with an accuracy of 0.65%.

Preparation of the Microchannel T-shaped Junction

The microchannel T-shaped junction is fabricated using wet etching on a glass substrate, measuring 30×60 mm^2, on which a 145 nm layer of chrome and a 570 nm layer of positive photoresist are

*Address correspondence to this author at the Department of Mechanical Engineering, The University of Hong Kong, Pokfulam Road, Hong Kong; Tel: +852 28597908; E-mail: lqwang@hku.hk

1573-4137/09 $55.00+.00 © 2009 Bentham Science Publishers Ltd.

Table 1. Measured Values of Continuous Phase Viscosity and Interfacial Tension

Disperse Phase-Continuous Phase	μ_c / mPa·s	σ / mN/m
Hexadecane-Deionized water	1.0	44.0
Hexadecane-30 wt.% glycerin aqueous solution	2.39	29.7
Hexadecane-60 wt.% glycerin aqueous solution	10.5	27.9
Hexadecane-0.0001 wt.% Tween 20 aqueous solution	1.0	28.0
Hexadecane-0.1 wt.% Tween 20 aqueous solution	1.0	10.0

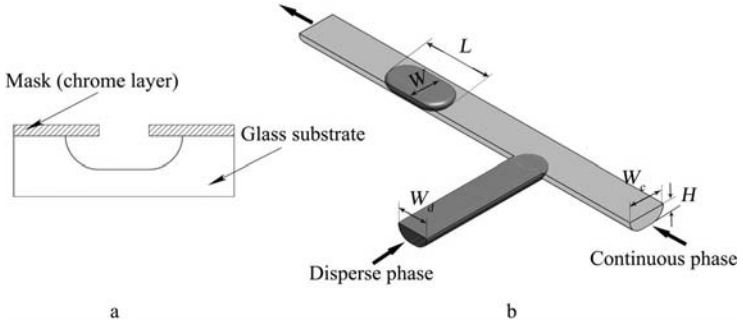

Fig. (1). Microfluidic T-shaped junction (**a**: the bow-like shape of the cross section of microchannels etched on glass substrate; **b**: one droplet formed in a microfluidic T-junction).

deposited (SG2506, Shaoguang Chrome Blank Co., Ltd., China). The pattern of the T-shaped junction printed on a film mask (Shenzhen New Way electronics Co. Ltd.) is transferred onto the photoresist layer after UV exposure in a UV exposure unit (LV204, Mega Electronics Ltd., UK). After development and chromium removing, the microchannel T-shaped junction is then etched on a glass substrate in a mixing solution of HF and NH4F (1 mol/L) in an ultrasonic environment at room temperature (Cole-Parmer® 8893, Cole-Parmer Instrument Company, USA). Another piece of clean glass plate with the same size is used to seal the microchannels by thermal bonding in a programmable Muffle furnace after desiccation in a vacuum oven (Vulcan® 3-550, DENTSPLY Ceramco, USA; DZF-6020, Shanghai Shengxin Scientific Instrument Factory, China). The cross section of the microchannel etched on glass material has a bow-like shape (Fig. (**1a**)), and the two asymmetric quarter-circles are resulted from the isotropic property of glass material in etching process. The glass surface exposed to the etchant is gradually etched from top to bottom in wet etching process. At the same time, the etching inside glass material also occurs in all other directions with an identical etching rate due to its isotropic property. The channel width continuously increases as the channel depth deepens, and the top portion of the channel cross-section has a wider width than the bottom portion because the upper portion experiences longer exposure time to the etchant (Fig. (**1a**)). Therefore, we have a bow-like cross section with wider top edge and shorter bottom edge.

The cross section area of disperse phase channel and continuous phase channel are calculated as:

$$A_d = (W_d - 2H)H + \frac{\pi H^2}{2} \quad (1)$$

and,

$$A_c = (W_c - 2H)H + \frac{\pi H^2}{2}, \quad (2)$$

where W_d is the wider width of disperse phase channel, W_c is the wider width of continuous phase channel, and H is the channel depth. Fig. (**1b**) shows a schematic diagram of the T-shaped junction having a uniform depth H of 35.4 μm. The continuous phase channel W_c has a value of 101.3 μm and the disperse phase channel width W_d is 86.5 μm. W_c and W_d are measured by using a vision measuring machine, and the channel depth H is measured by using a surface roughness tester (Quick Vision Pro 202; SV-3000S4. Mitutoyo Corporation, Japan).

Experimental Setup

Fig. (**2**) illustrates the experimental system. The disperse phase and the continuous phase are injected into the T-shaped junction by two syringe pumps via flexible PTFE tubing (Cole-Parmer Instrument Company, USA). Flow rate of either phase is automatically controlled by the syringe pump. When the two flow streams meet at the T-shaped junction, droplets will be formed as a result of the interaction between the two phases. An inversed microscope is used for visualization purpose (XD101, Nanjing Jiangnan Novel Optics Co. Ltd., China), with which a high speed camera is integrated for recording the droplet formation process in terms of images and videos (MotionPro® X4, IDT, Taiwan). Droplet formation time is directly measured from the consecutive images by utilizing the software with the high speed camera. Droplet volume can be derived from the dimensions and area of droplets in the images in Adobe Photoshop, together with the geometrical characteristics of the continuous phase channel. To ensure droplet formation time and droplet volume are collected under a steady state flow, we check out the number of droplets formed within a specific time period at least three times with a 5 minutes interval after every change of either disperse phase flow rate or continuous phase flow rate. We collect data of the droplet formation time and droplet volume only when the number does not change for the last two measurements.

RESULTS AND DISCUSSION

Nanoliter Droplet Formation Process

Two stages have been identified during a typical nanoliter droplet formation process: (1) the growing stage—when the two streams meet at the T-shaped junction, the disperse phase tip gradually in-

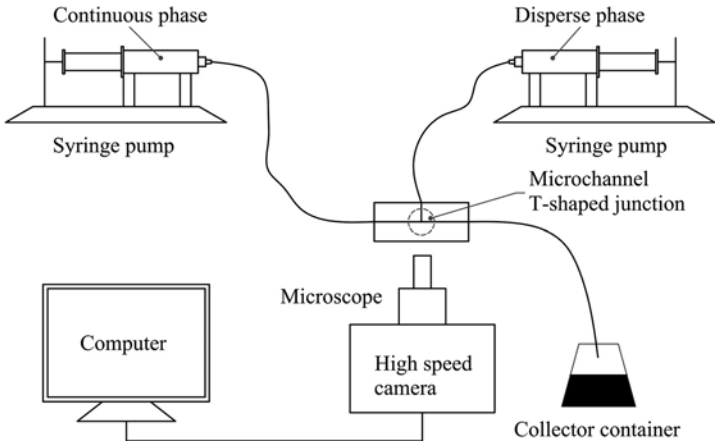

Fig. (2). Experimental system setup.

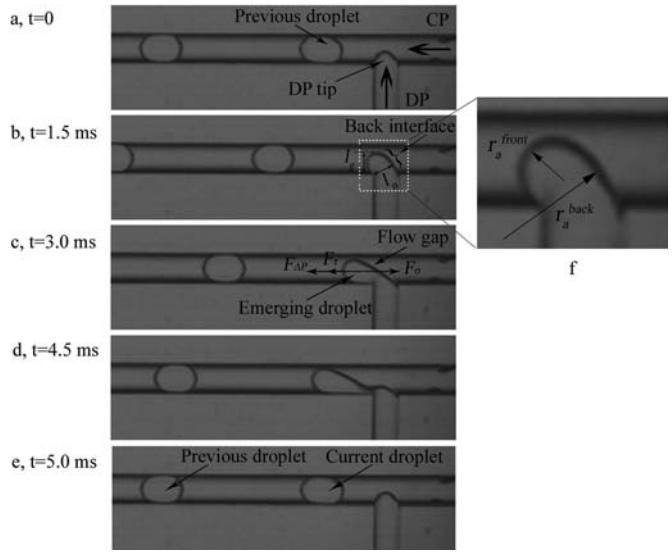

Fig. (3). Photo sequence showing typical formation process of droplets (CP: continuous phase, 0.1 wt.% Tween 20 aqueous solution; DP: disperse phase, hexadecane; $Q_c = 16$ μL/m, $Q_d = 6$ μL/m).

trudes and inflates into the continuous phase (Figs. (**3a, b**)) and reaches a critical position after which the back interface of disperse phase tip starts travelling downstream (Fig. (**3b**)), and (2) the necking stage—after reaching the critical position, the back interface moves downstream in the continuous phase, and the neck connecting the forming droplet and disperse main stream becomes thinner and thinner until it breaks near the downstream corner of the T-shaped junction (Fig. (**3c-e**)). In either growing or necking stage, the forming droplet is confined by the walls of continuous phase channel, but does not wet channel walls because there always exists a thin layer of continuous phase between the forming interface and channel walls, resulted from the higher surface energy between water and glass walls than that between hexadecane and glass walls. Although the cross section of the microchannel is bow-like, we do not find evident difference on the droplet formation process compared with that for rectangular T-shaped junctions in [27], which implies that the mechanism of droplet formation in these two cases should be the same. The existence of the thin layer continuous phase weakens the influence of curved side walls. Therefore droplet formation time and droplet volume reported in the present work should also be applicable to T-shaped junctions of rectangular microchannels.

Droplet Volume Determination

As shown in Fig. (**1a**), because of the irregular cross section of the microchannel, precise determination of droplet volume is a crucial issue. We measured droplet length, droplet width and droplet area in Adobe Photoshop as indicated in Fig. (**1b**), and found that most of the droplets in our experiment are longer than the width of continuous phase channel. In such a situation, it is reasonable to assume the middle part of a long droplet fully occupies the cross section of continuous phase channel, and the two ends have the same diameter as continuous phase channel width in horizontal plane and have the same curved tip as the curved wall of continuous phase channel has in the plane of cross section. With the above postulations, we calculate the droplet volume based on our measurements as:

$$V_{dr} = H\left(L - W_c\right)\left(W_c - \frac{H\left(4-\pi\right)}{2}\right) + \pi H\left(H^2\left(\frac{W_c - 2H}{4} + \frac{2}{3}\right) + \frac{\left(W_c - 2H\right)^2}{4}\right) \quad (3)$$

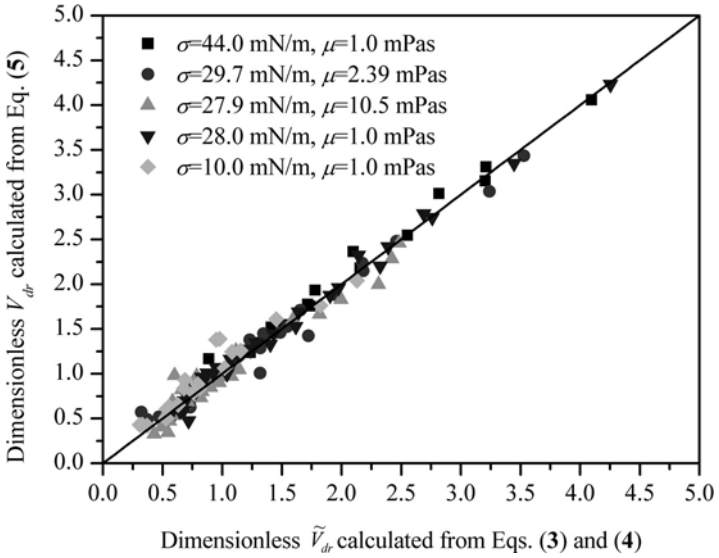

Fig. (4). Comparison between dimensionless volume $\widetilde{V}_{dr}$ calculated from Eqs. (3) and (4) and that from Eq. (5), $\widetilde{V}_{dr} = V_{dr} / W_c W_d H$.

where *L* is droplet length between its two ends. Note that Eq. (3) is valid only for the case $L \geq W_c$. When $L < W_c$, we assume that the droplet has a "cylindrical" shape confined by the continuous channel depth. In this situation, V_{dr} is calculated by

$$V_{dr} = \kappa A_{dr} H, \tag{4}$$

where *k* is the correction coefficient used to modify the cylindrical assumption, A_{dr} is the droplet area measured in Adobe Photoshop. When $L = W_c$, the value of *k* can be derived from Eq. (3), which is equal to 0.83. For the case of $L < W_c$, we estimate that *k* value does not vary too much because the droplet generated in our experiment is not smaller than W_c too much, usually larger than half W_c. In fact, the droplet volume is slightly smaller than the value of "cylindrical droplet" considering the bended edges in reality. So a constant value $k = 0.80$ is accepted in Eq. (4) when $L \leq W_c$. The volume of nanoliter droplets generated in our experiment locates between 0.10 to 1.32 nL (nano Liter) calculated by Eqs. (3) and (4).

Validation of the Relation Between Droplet Formation Time and Droplet Volume

For an incompressible disperse phase, the droplet volume should be equal to the volume of disperse phase flowed into the tip within droplet formation time. Since the disperse phase flows at constant flow rates in our experiment, the droplet volume can be calculated as:

$$V_{dr} = t_{dr} \cdot Q_d, \tag{5}$$

where t_{dr} represents the droplet formation time, and Q_d is the disperse phase flow rate. We make a comparison of the droplet volume determined by Eqs. (3) and (4) to that calculated by Eq. (5) in Fig. (**4**) in a dimensionless format. In Fig. (**4**) the droplet volume V_{dr} is normalized by $W_c W_d H$. The good agreement shows that Eqs. (3) and (4) are effective and accurate for determining the droplet volume. It is also confirmed that Eq. (5) is safe to be used to relate the droplet volume with the droplet formation time.

Analysis of Droplet Formation Time

Droplet formation time consists of two parts: the time consumed in the growing stage and the time consumed in the necking stage. The former is:

$$t_g = \frac{l_g}{\bar{v}_g}, \tag{6}$$

where l_g is the distance of the disperse tip penetrated into continuous phase in the growing stage (Fig. (**3b**)), and $\bar{v}_g$ is the average intrusion speed of the disperse tip penetrating into the continuous phase in the growing stage. In the growing stage, the disperse phase tip does not too much inflate into the continuous phase downstream, which leads to $\bar{v}_g$ approximation by v_d, the mean velocity of the disperse phase flowing in disperse phase channel. The penetration length l_g is always less than but comparable with W_c as found by experimental visualization of droplet formation process. In Eq. (6), using W_c instead of l_g will overvalue t_g since the disperse phase can hardly block the entire width of the continuous phase channel in the growing stage, resulting in $l_g < W_c$; and using v_d instead of $\bar{v}_g$ will underestimate t_g because in the growing stage the front interface does inflate downstream a little into the continuous phase, resulting in $\bar{v}_g < v_d$. Because of this two-side effect, W_c / v_d should give a reasonable estimation of t_g. Considering the influence of fluids properties, a correction coefficient *a* that should be on the order of one is used to correct W_c / v_d. Therefore t_g is calculated by:

$$t_g = a \frac{W_c}{v_d}, \tag{7}$$

where *a* is the dimensionless correction coefficient, and v_d is calculated by:

$$v_d = \frac{Q_d}{A_d}. \quad (8)$$

Here Q_d is the volumetric flow rate of the disperse phase. During the fitting of experimental data, the value of *a* is verified on the order of one.

The necking time taken by the back interface travelling from the critical position to breakup point is:

$$t_n = \frac{l_n}{\bar{v}_n}, \quad (9)$$

where l_n is the distance that back interface travels in the necking stage (Fig. (**3b**)), $\bar{v}_n$ is the average speed of the back interface travelling downstream in continuous phase channel during the necking stage. Based on the visualization of droplet formation process, l_n can be approximated by W_d. The average travelling speed $\bar{v}_n$ has a same magnitude of v_c the mean velocity of continuous phase flowing in the continuous phase channel. In Eq. (9), using W_d in place of l_n will overestimate t_n because $W_d > l_n$, and using v_c in place of $\bar{v}_n$ will underestimate t_n because $v_c > \bar{v}_n$ due to the leakage flow of continuous phase between the disperse tip and channel walls. Because of this two-side effect, W_d / v_c should give a reasonable estimation of t_n. For the same reason as calculating t_g, a correction coefficient *b* is adopted to calculate t_n which is evaluated by:

$$t_n = b\frac{W_d}{v_c}, \quad (10)$$

where *b* is a dimensionless correction coefficient, v_c is calculated by:

$$v_c = \frac{Q_c}{A_c}. \quad (11)$$

In Eq. (11), Q_c is volumetric flow rate of disperse phase. During fitting of experimental data, the value of *b* is verified on the order of one.

To find how *a* and *b* correct the estimation of time consumed in the two stages, a detailed investigation of main forces interacting between interface and continuous phase in the T-shaped junction is essential, though force balance model could not give the result directly. In unconfined T-shaped junctions, the disperse phase tip grows, deforms and breaks under a series of forces all of which can be clarified as two groups depending on the effect of forces on droplet formation: first, holding force trying to stabilize the forming droplets on the orifice of disperse phase channel, which includes interfacial tension force only; second, detaching forces trying to detach the forming droplets, which include buoyancy force caused by density difference and gravity, viscous force exerted by continuous phase flow, and inertial force caused by disperse phase flow and inflation [25, 26]. Force analysis in confined T-shaped junctions is much more difficult than in unconfined T-shaped junctions because of the highly disturbed flow field of continuous phase around the confined, developing droplets, even though some work has been reported [24, 27, 32]. For the confined T-shaped junction in our experiment, droplets formation occurred in the horizontal plane only, and then any force perpendicular to this plane does not contribute to the droplet detachment, which excludes the buoyancy force as the leading force. In fact, buoyancy force can be omitted in our situation because of the small density difference between hexadecane and water. Inertial force caused by disperse phase flow moving through the continuous phase channel as it inflates the droplet is negligible, since the Reynolds number of disperse phase is much smaller than unity $Re = \rho_d v_d H / \mu_d << 1$. In the horizontal plane, the growing droplets are confined by side walls of continuous phase channel, and detach along the direction of continuous phase flow. So, any possible forces along disperse phase channel can be neglected and only possible forces along continuous phase channel are considered. Along continuous channel, there are three forces playing roles on determining droplet formation—interfacial tension force $F_\sigma \propto \sigma$, viscous force $F_\tau \propto \mu_c v_c$ and the force arising from pressure difference over the forming droplet $F_{\Delta P} \propto \mu_c v_c$ [27]. The interfacial tension force is associated with the Laplace pressure jump across a static or quasi-static curved interface, $\Delta P = \sigma\left(r_a^{-1} + r_r^{-1}\right)$ where r_a is the radius of the curved interface in the horizontal plane, r_r is the radius of the curved interface in the plane of vertical section of continuous phase channel. Since the forming droplet is confined by the up and bottom walls of continuous phase channel, the radii of the curved front and back interfaces are identical and equal to half channel depth, $r_r = H/2$. The front interface has a much more curved interface than the back interface has in the horizontal plane $r_a^{front} < r_a^{back}$ (Fig. (**3f**)), which resulted in the pressure jump across the front interface, pointing upstream, larger than the pressure jump across the back interface, pointing downstream. so, the resultant force caused by pressure jump at front and back interfaces is pointing upstream, the opposite direction of droplet detachment as shown in Fig. (**3c**), given the pressure inside the growing droplet is identical everywhere. Unlike in unconfined T-shaped junctions, the force caused by pressure difference between the back and the front interface of the forming droplets in continuous phase is not negligible but comparable with the viscous force in the confined T-shaped junction because of the high flow resistance due to the blockage of forming droplets [27]. In the growing stage, with the penetration of disperse phase tip, the continuous phase pressure behind the back interface rises rapidly due to the sharp reduction of the flow gap in continuous phase channel as shown in Fig. (**3b**). The viscous stress exerted on the interface also builds up because of the increase of continuous phase velocity flowing through the gap. When the pressure and viscous stress are high enough, the back interface stops expanding upstream in continuous phase, and starts to travel downstream in the continuous flow, and the droplet formation process enters the necking stage. In the necking stage, the back interface accelerates from zero velocity under the forces F_τ and $F_{\Delta P}$ exerted by the continuous phase. Increase, either in continuous phase velocity v_c or in continuous phase viscosity μ_c, will shorten time t_g and t_n, because of the increased F_τ and $F_{\Delta P}$ exerted on the interface. In the droplet formation process, interfacial tension force F_σ is the only force that stabilizes the emerging droplet. Increased interfacial tension will elongate the time consumed in both stages due to the enhanced stabilization effect. From the analysis above, no matter which detaching force is playing leading role on droplet formation, either detaching force is proportional to the product of $\mu_c v_c$, and the only

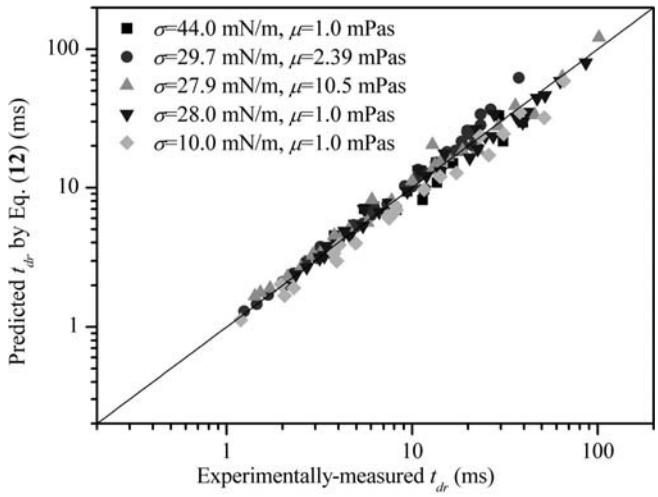

Fig. (5). Comparisons between experimentally-measured t_{dr} and that calculated by Eq. (12).

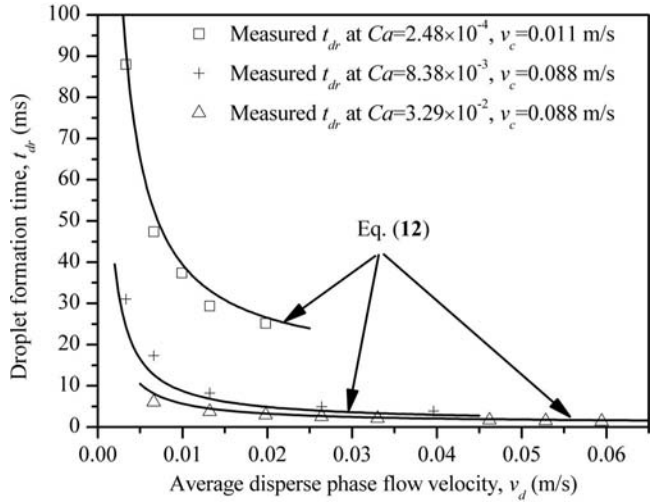

Fig. (6). Comparison between experimentally-measured t_{dr} and that predicted by Eq. (12) as a function of v_d.

stabilization force is proportional to the interfacial tension σ. It, then, can be interpreted as $\mu_c v_c$ and σ affect the droplet formation time most considerably among other parameters in opposite directions. Therefore it is reasonable to conclude the capillary number $Ca = \mu_c v_c / \sigma$ to dominate the format of *a* and *b*, the correction coefficients in characterizing t_g and t_n. Then the droplet formation time t_{dr} is proposed to have a form of:

$$t_{dr} = C_g \cdot Ca^{\alpha} \frac{W_c}{v_d} + C_n \cdot Ca^{\beta} \frac{W_d}{v_c} \tag{12}$$

where C_g, C_n, α and β are, dimensionless constants that depend on geometrical characteristics of the T-shaped junctions. For the T-shaped junction used in our experiment, we find that $C_g = 0.147$, $\alpha = -0.344$, $C_n = 0.535$ and $\beta = -0.141$ by fitting our experimental data. We compare the droplet formation time measured in the experiment with that predicted by Eq. (12) in Fig. (**5**), which is showing that Eq. (12) works very well. The measured droplet formation time and that predicted by Eq. (12) are also compared as the function of v_d and Ca in Figs. (**6**) and (**7**), respectively. The good agreement confirms our analysis of droplet formation process and the validity of Eq. (12) for predicting the droplet formation time, though the explicit relations between geometrical characteristics and C_g, C_n, α and β are still unclear.

Droplet Volume

By Eqs. (12) and (5), the droplet volume can be obtained by:

$$V_{dr} = C_g \cdot Ca^{\alpha} W_c A_d + C_n \cdot Ca^{\beta} W_d A_c \frac{Q_d}{Q_c} \tag{13}$$

Therefore, the dimensionless droplet volume is, after dividing Eq. (13) by $W_c W_d H$,

$$\tilde{V}_{dr} = \frac{V_{dr}}{W_c W_d H} = C_g \cdot Ca^{\alpha} \frac{A_d}{W_d H} + C_n \cdot Ca^{\beta} \frac{A_c}{W_c H} \frac{Q_d}{Q_c}, \tag{14}$$

where $A_d / W_d H$ and $A_c / W_c H$ are solely dependent on the shape and dimension of the cross section of microchannels, and are equal to 0.82 and 0.85 for the disperse phase channel and the continuous phase channel in our experiment, respectively. Comparison of the droplet volume experimentally measured and predicted by Eq. (14)

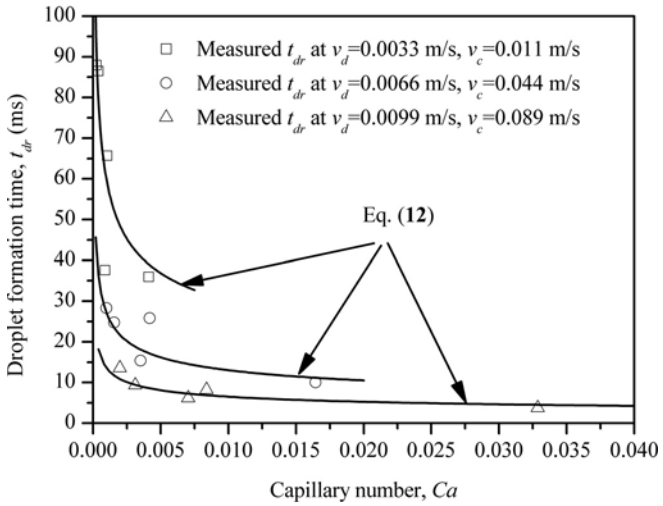

Fig. (7). Comparison between experimentally-measured t_{dr} and that predicted by Eq. (12) as a function of Ca.

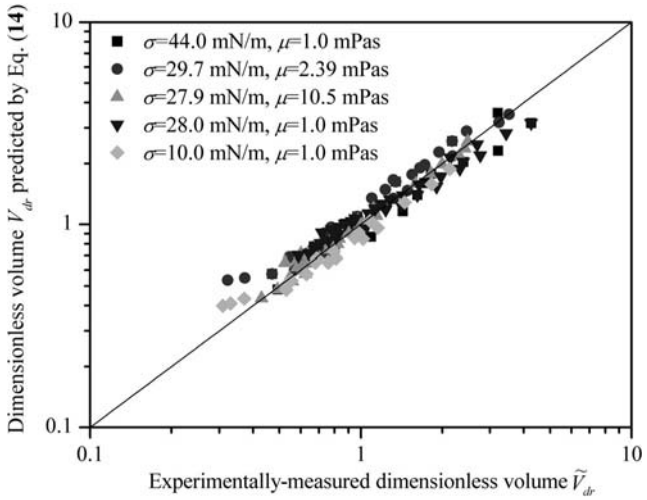

Fig. (8). Comparison between experimentally-measured $\tilde{V}_{dr}$ and that predicted by Eq. (**14**), $\tilde{V}_{dr} = V_{dr} / W_c W_d H$.

is shown in Fig. (**8**); the good agreement reveals the high accuracy of Eq. (14) to predict droplet volume.

On the right side of Eq. (14), the first item varies from 2.10 to 0.39 and the second item except Q_d / Q_c varies from 1.46 to 0.74 when Ca changes in our experimental arrange ($2.5\times10^{-4} < Ca < 3.3\times10^{-2}$). The unity order of these two values exhibits the consistency of our result with the reported scaling analysis of dimensionless volume of droplets generated in confined T-shaped junctions, which is

$$\tilde{V}_{dr} = 1 + \lambda \frac{Q_d}{Q_c} \tag{15}$$

where λ is a constant of order unity and only depends on the geometrical characteristics of T-shaped junctions [27, 32]. However, in our experiment for a specific T-shaped junction, the value of λ changes a lot from our experiment results, 171% increase from 0.7 to 1.9, and, in addition to Q_d / Q_c, Ca has also been found having a strong influence on the droplet volume. The influence of Ca is also reported by *van der Graaf et al.* and stated as:

$$V_{dr} = V_{crit,ref} Ca^m + t_{neck,ref} Ca^n Q_d \tag{16}$$

where $V_{crit,ref}$ is the critical volume at $Ca = 1$, $t_{neck,ref}$ is the necking time at $Ca = 1$ [33]. The exponents *m* and *n* depend on the geometrical characteristics of the T-shaped junction, and are taken to be $m = n = -0.75$ for the T-shaped junction the author used with square cross section measuring 100×100 μm^2. Although λ in Eq. (15) and the exponent *m* and *n* in Eq. (16) were reported depending on the geometrical characteristics of T-shaped junctions only, the explicit dependency is still an open question. It is noted that, from Eqs. (15) and (16) and our results, both flow rate ratio Q_d / Q_c and Ca play important roles on determining droplet volume generated in confined T-shaped junctions.

CONCLUDING REMARKS

Nanoliter droplet formation in a confined T-shaped junction is experimentally analyzed. The movement of the back interface of the tip of disperse phase plays a very important role in determining droplet formation time and droplet volume. A simple model for predicting the droplet formation time is developed based on experimental discoveries and force analysis during droplet formation. The droplet formation time is a sum of two parts: the time required for growing and the time taken for necking. The former is mainly governed by the mean velocity of disperse phase, and the latter is

mainly determined by the mean velocity of continuous phase. It is experimentally confirmed that the droplet volume is equal to the volume of disperse phase flowed into the tip within droplet formation time. Influences of continuous phase viscosity and interfacial tension, together with the mean velocity of continuous phase, can be characterized by Capillary number Ca as a correction coefficient to predict droplet formation time and droplet volume. From Eq. (12) it is shown that the droplet formation time decreases as either Capillary number or mean velocity of continuous phase or mean velocity of disperse phase increases. Both Capillary number Ca and flow rate ratio Q_d / Q_c are found to have strong influences on droplet volume formed in the confined T-shaped junction. Although the dependency of C_g, C_n, α and β on geometrical characteristics of T-shaped junctions are not explored in our model, the format of Eq. (14) should be more accurate and general to predict droplet volume as it considers both influences of Ca and Q_d / Q_c.

ACKNOWLEDGEMENTS

The financial support from the CRCG of the University of Hong Kong (10207238 and 10207923) and the Research Grants Council of Hong Kong (GRF718009) is gratefully acknowledged.

REFERENCES

[1] Clausell-Tormos, J.; Lieber, D.; Baret, J.C.; El-Harrak, A.; Miller, O.J.; Frenz, L.; Blouwolff, J.; Humphry, K.J.; Koster, S.; Duan, H.; Holtze, C.; Weitz, D.A.; Griffiths, A.D.; Merten, C.A. Droplet-based microfluidic platforms for the encapsulation and screening of mammalian cells and multicellular organisms. *Chem. Biol.*, **2008**, *15*(5), 427-437.

[2] Henares, T.G.; Mizutani, F.; Sekizawa, R.; Hisamoto, H. Single-drop analysis of various proteases in a cancer cell lysate using a capillary-assembled microchip. *Anal. Bioanal. Chem.*, **2008**, *391*(7), 2507-2512.

[3] Li, S.W.; Xu, H.H.; Wang, Y.J.; Luo, G.S. Controllable preparation of nanoparticles by drops and plugs flow in a microchannel device. *Langmuir*, **2008**, *24*(8), 4194-4199.

[4] Song, Y.J.; Hormes, J.; Kumar, C. Microfluidic synthesis of nanomaterials. *Small*, **2008**, *4*(6), 698-711.

[5] Chan, E.M.; Alivisatos, A.P.; Mathies, R.A. High-temperature microfluidic synthesis of cdse nanocrystals in nanoliter droplets. *J. Am. Chem. Soc.*, **2005**, *127*(40), 13854-13861.

[6] Hung, L.H.; Choi, K.M.; Tseng, W.Y.; Tan, Y.C.; Shea, K.J.; Lee, A.P. Alternating droplet generation and controlled dynamic droplet fusion in microfluidic device for cds nanoparticle synthesis. *Lab Chip*, **2006**, *6*(2), 174-178.

[7] Shestopalov, I.; Tice, J.D.; Ismagilov, R.F. Multi-step synthesis of nanoparticles performed on millisecond time scale in a microfluidic droplet-based system. *Lab Chip*, **2004**, *4*(4), 316-321.

[8] Song, H.; Chen, D.L.; Ismagilov, R.F. Reactions in droplets in microflulidic channels. *Angew. Chem. Int. Ed.*, **2006**, *45*(44), 7336-7356.

[9] Kobayashi, I.; Nakajima, M. Microchannel emulsification technology: Formulation and application of monodisperse emulsions. *J. Jpn. Soc. Food Sci. Technol. Nippon Shokuhin Kagaku Kogaku Kaishi*, **2006**, *53*(6), 317-326.

[10] Kawakatsu, T.; Komori, H.; Nakajima, M.; Kikuchi, Y.; Yonemoto, T. Production of monodispersed oil-in-water emulsion using crossflow-type silicon microchannel plate. *J. Chem. Eng. Jpn.*, **1999**, *32*(2), 241-244.

[11] Kobayashi, I.; Lou, X.F.; Mukataka, S.; Nakajima, M. Preparation of monodisperse water-in-oil-in-water emulsions using microfluidization and straight-through microchannel emulsification. *J. Am. Oil Chem. Soc.*, **2005**, *82*(1), 65-71.

[12] Saito, M.; Yin, L.J.; Kobayashi, I.; Nakajima, M. Preparation characteristics of monodispersed oil-in-water emulsions with large particles stabilized by proteins in straight-through microchannel emulsification. *Food Hydrocolloids*, **2005**, *19*(4), 745-751.

[13] Xu, Q.Y.; Nakajima, M.; Binks, B.P. Preparation of particle-stabilized oil-in-water emulsions with the microchannel emulsification method. *Colloids Surf. A*, **2005**, *262*(1-3), 94-100.

[14] Anna, S.L.; Bontoux, N.; Stone, H.A. Formation of dispersions using "Flow focusing" In microchannels. *Appl. Phys. Lett.*, **2003**, *82*(3), 364-366.

[15] Ganan-Calvo, A.M. Perfectly monodisperse microbubbling by capillary flow focusing: An alternate physical description and universal scaling. *Phys. Rev. E*, **2004**, *69*(2), 027301.

[16] Ganan-Calvo, A.M.; Gordillo, J.M. Perfectly monodisperse microbubbling by capillary flow focusing. *Phys. Rev. Lett.*, **2001**, *87*(27), 274501.

[17] Garstecki, P.; Gitlin, I.; DiLuzio, W.; Whitesides, G.M.; Kumacheva, E.; Stone, H.A. Formation of monodisperse bubbles in a microfluidic flow-focusing device. *Appl. Phys. Lett.*, **2004**, *85*(13), 2649-2651.

[18] Garstecki, P.; Stone, H.A.; Whitesides, G.M. Mechanism for flow-rate controlled breakup in confined geometries: a route to monodisperse emulsions. *Phys. Rev. Lett.*, **2005**, *94*(16), 164501.

[19] Chu, L.Y.; Utada, A.S.; Shah, R.K.; Kim, J.W.; Weitz, D.A. Controllable monodisperse multiple emulsions. *Angew. Chem. Int. Ed.*, **2007**, *46*(47), 8970-8974.

[20] Shah, R.K.; Shum, H.C.; Rowat, A.C.; Lee, D.; Agresti, J.J.; Utada, A.S.; Chu, L.Y.; Kim, J.W.; Fernandez-Nieves, A.; Martinez, C.J.; Weitz, D.A. Designer emulsions using microfluidics. *Mater. Today*, **2008**, *11*(4), 18-27.

[21] Utada, A.S.; Lorenceau, E.; Link, D.R.; Kaplan, P.D.; Stone, H.A.; Weitz, D.A. Monodisperse double emulsions generated from a microcapillary device. *Science*, **2005**, *308*(5721), 537-541.

[22] Xu, J.H.; Li, S.W.; Tan, J.; Wang, Y.J.; Luo, G.S. Controllable preparation of monodisperse o/w and w/o emulsions in the same microfluidic device. *Langmuir*, **2006**, *22*(19), 7943-7946.

[23] van der Graaf, S.; Steegmans, M.L.J.; van der Sman, R.G.M.; Schroen, C.; Boom, R.M. Droplet formation in a t-shaped microchannel junction: A model system for membrane emulsification. *Colloids Surf. A*, **2005**, *266*(1-3), 106-116.

[24] Thorsen, T.; Roberts, R.W.; Arnold, F.H.; Quake, S.R. Dynamic pattern formation in a vesicle-generating microfluidic device. *Phys. Rev. Lett.*, **2001**, *86*(18), 4163-4166.

[25] Husny, J.; Cooper-White, J.J. The effect of elasticity on drop creation in t-shaped microchannels. *J. Non-Newtonian Fluid Mech.*, **2006**, *137*(1-3), 121-136.

[26] Xu, J.H.; Luo, G.S.; Chen, G.G.; Wang, J.D. Experimental and theoretical approaches on droplet formation from a micrometer screen hole. *J. Membr. Sci.*, **2005**, *266*(1-2), 121-131.

[27] Garstecki, P.; Fuerstman, M.J.; Stone, H.A.; Whitesides, G.M. Formation of droplets and bubbles in a microfluidic t-junction - scaling and mechanism of break-up. *Lab. Chip*, **2006**, *6*(3), 437-446.

[28] Xu, J.H.; Li, S.W.; Tan, J.; Wang, Y.J.; Luo, G.S. Preparation of highly monodisperse droplet in a t-junction microfluidic device. *AIChEJ*, **2006**, *52*(9), 3005-3010.

[29] Christopher, G.F.; Anna, S.L. Microfluidic methods for generating continuous droplet streams. *J. Phys. D Appl. Phys.*, **2007**, *40*(19), R319-R336.

[30] De Luca, G.; Drioli, E. Force balance conditions for droplet formation in cross-flow membrane emulsifications. *J. Colloid Interface Sci.*, **2006**, *294*(2), 436-448.

[31] Peng, S.J.; Williams, R.A. Controlled production of emulsions using a cross-flow membrane. *Part Part. Syst. Char.*, **1998**, *15*(1), 21-25.

[32] De Menech, M.; Garstecki, P.; Jousse, F.; Stone, H.A. Transition from squeezing to dripping in a microfluidic t-shaped junction. *J. Fluid Mech.*, **2008**, *595*, 141-161.

[33] van der Graaf, S.; Nisisako, T.; Schroen, C.; van der Sman, R.G.M.; Boom, R.M. Lattice boltzmann simulations of droplet formation in a t-shaped microchannel. *Langmuir*, **2006**, *22*(9), 4144-4152.

Received: May 04, 2009 Revised: June 06, 2009 Accepted: June 08, 2009